Radar Measurements at 16.5 GHz in the Oceanic Evaporation Duct

KENNETH D. ANDERSON

Abstract—**A unique series of radar measurements demonstrates that a 16.5-GHz radar, located at typical shipboard antenna heights, can effectively exploit the existence of the oceanic evaporation duct to achieve surface ship detection ranges of more than twice the standard horizon range. Observations of surface targets of opportunity made at two sites on the U.S. Pacific coast from July 1984 through January 1986 agree with predictions from a simple propagation model. This model combines a single-mode waveguide approximation with a model of the surface target's radar cross-section distribution to determine the maximum radar detection range for various evaporation duct heights. A frequency distribution of predicted detection range is given, based on the evaporation duct climatology for two locations. Although the radar measurements and the predictions are for a specific frequency, it is highly probable that the model can be extended to predict the performance of surface-search radars operating at other frequencies and in other areas of the ocean.**

I. Introduction and Background

PROPAGATION OF RADIO WAVES near the ocean surface can be separated into two classes, standard and nonstandard. Standard propagation is associated with the so-called standard atmosphere in which, at low altitudes, the radio refractive index decreases linearly with height [1]. Nonstandard propagation is associated with abnormal vertical distributions of the refractive index [2]. The most dramatic nonstandard effects are those caused by ducting, which can result in propagation ranges far exceeding the normal horizon.

In a marine environment there are three types of ducts: surface-based ducts, elevated ducts, and evaporation ducts. Surface-based and elevated ducts are formed by subsidence or advection of differing air masses and can be several hundred meters thick. These ducts are comparatively frequency insensitive and can support long propagation ranges for frequencies as low as 100 MHz. The evaporation duct is created by the logarithmic decrease of water vapor in the first several meters above the ocean surface. It is a nearly permanent ducting mechanism, affecting frequencies as low as 3 GHz [3]–[5]. The evaporation duct height δ defines the strength of the mechanism and is determined by surface meteorological measurements [6]–[8].

In 1981–1982 an experiment was performed to investigate evaporation duct effects at 17.7 GHz. A propagation path between two southern California coastal islands, separated by 81 km, was instrumented to record path loss (ratio of transmitted power to received power for isotropic antennas) and δ. The transmitter was 20 m above msl and the receiver was 18.8 m above msl. In a standard atmosphere, tropospheric scatter [9] is the dominant propagation mechanism for the geometry and predicts a path loss of 225 dB. Fig. 1 is a scatter diagram of observed path loss and δ for a three-week period in June 1982 and amply illustrates the ability of the evaporation duct to support high signal levels at moderate over-the-horizon ranges.

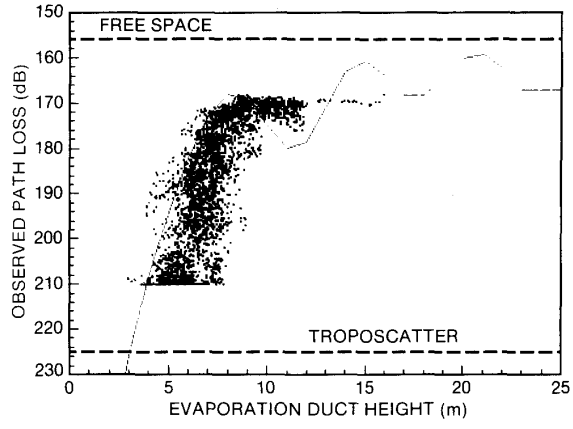

Fig. 1. Observed path loss for evaporation duct conditions at 17.7 GHz during June 1982. Troposcatter level is 225 dB.

In 1983, an analytical effort examined the effects of evaporation ducting on shipboard surface-search radars [10]. A global evaporation duct height climatology [11] was used to predict the probability of detecting surface targets at ranges well beyond the normal radar horizon. Four radar frequencies were considered: 3, 6, 10, and 18 GHz. Predicted radar performance is summarized in Fig. 2. Although the 1981–1982 experimental data strongly supports the prediction techniques, actual radar data were not available when the analysis was completed. Therefore, the experiment discussed in this paper was developed to achieve two purposes:

1) to demonstrate the enhanced surface target detection ranges due to the evaporation duct;
2) to obtain sufficient radar and meteorological data to validate the prediction model.

II. Experiment Description

A. Radar

To assess the effects of the evaporation duct on shipboard radar detection of surface-ship targets and to assess the validity

Manuscript received October 26, 1987.
The author is with the Naval Ocean Systems Center, Code 543, San Diego, CA 92152-5000.
IEEE Log Number 8824100.

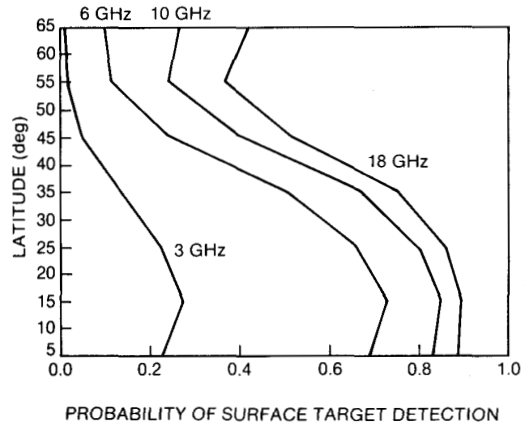

Fig. 2. Geographic influence of the evaporation duct on shipboard radar detection of a ship well beyond the standard radar horizon.

of the prediction techniques, a series of measurements were made with a 16.5-GHz radar at two sites on the U.S. Pacific coast. From July 1984 to April 1985, radar measurements were made in San Diego (SD site) at the Naval Ocean Systems Center (NOSC). The radar was located 22.9 m above msl and 27 days of measurements were made. The radar was then moved to a coastal site in the state of Washington (WC site) to collect data in an environment different from that in the SD area. The radar was located 38.1 m above msl. Measurements began in August 1985 and continued through January 1986; nine days of measurements were completed.

Radar characteristics are listed in Table I. A digital noncoherent integrator provided a free-space detection range of 40.9 nm for a 1 m^2 cross-section target. The integrator was clocked at 2 MHz and had two independent 2048-word by 16-bit memories. One memory accumulated the digitized (eight-bit) receiver video, while the second memory accumulated the single-bit result from a programmable threshold comparator. Software was written to examine the range/amplitude data in groups of 16 consecutive range cells and extract the maximum amplitude. Thus, the minimum range resolution was 0.65 nm. The final, compacted, range/amplitude data were displayed graphically in real-time and written to a disk file for post-operation analysis.

During operation at both sites, the radar was programmed to scan an azimuth sector from 180° to 329°. Starting at 180°, the antenna was positioned to point at the ocean horizon. After the requested number of pulses were processed by the integrator, the antenna positioner was stepped one degree (the antenna beamwidth) in azimuth. When the positioner stabilized, pulse integration was restarted for the new azimuth bearing. Once the antenna reached the end of the sector, it was swept back to the initial bearing, and a new scan was started.

B. Climatology and Environment

The National Climatic Data Center (NCDC), Asheville, NC, maintains a global data base of surface meteorological observations assembled from ship reports, from automatic buoys, and from foreign meteorological services [12]. Under

TABLE I
RADAR CHARACTERISTICS

Frequency	16500 MHz
Peak Power	100 KW
Pulse Length	600 ns
Pulse Rate	708 pps
Pulse Integration	128
Receiver Noise Figure	13 dB
Antenna Gain	44 dBi
Polarization	Vertical
Vertical Beamwidth	1 degree
Horizontal Beamwidth	1 degree
Scan Rate	Stepped

sponsorship from NOSC, NCDC analyzed a subset of its data base to produce a climatology of the evaporation duct height δ. This subset analysis, known as DUCT63, spans 15 years of surface observations, from 1970 through 1984, and covers nearly all ocean areas from 40° S to 70° N latitude [13]. The smallest geographical resolution within DUCT63 is a spatial region, 10° latitude by 10° longitude, known as a Marsden Square. In each Marsden Square, δ is distributed diurnally by month in intervals of 2 m from 0 m to 40 m. Similar distributions of other surface quantities, such as wind speed, absolute humidity and surface-to-surface attenuation rates at 35 and 94 GHz are included in the DUCT63 analysis.

The yearly mean δ distribution for the SD site is shown in Fig. 3(a). Approximately 59 000 surface ship observations were analyzed to compute this distribution. In San Diego, 80 percent of the observed δ are within the range of 4 to 16 m, 90 percent of the time duct heights are greater than 4 m, and the median δ is 9.1 m. This distribution may be compared to the one for the WC site (Fig. 3(b)) in which over 100 000 observations were analyzed. In the higher latitudes, lower δ are frequent; 30 percent of the observed δ are less than 4 m, 90 percent are less than 12 m, and the median is 6.6 m. All propagation predictions, described later, are derived from these two δ distributions.

Fig. 3(c) shows the worldwide yearly mean δ distribution for all Marsden Square data in the DUCT63 analysis. It is the average of all δ observed in ocean areas between 40° S and 70° N latitude over all 12 months without regard for day and night variations. It should be noted that 80 percent of the observed duct heights are within the range of 4 to 22 m. The median duct height is 13.1 m, which is greater than the median δ at the SD and WC sites. Therefore, on a worldwide basis, one can assume that the detection ranges would be greater than the ranges observed in the measurements.

The presence or absence of surface-based or elevated ducts created by processes other than surface flux of heat and moisture is determined by a radiosonde. As the radiosonde rises through the atmosphere, it telemeters measurements of pressure, temperature, and relative humidity to a ground station receiver. Although surface-based ducts from elevated layers typically occur 8 percent of the time [14], varying with location and season, these ducts may exist for days, even weeks. Radiosonde observations were routinely made during radar operations to isolate periods when the evaporation duct was the controlling ducting mechanism.

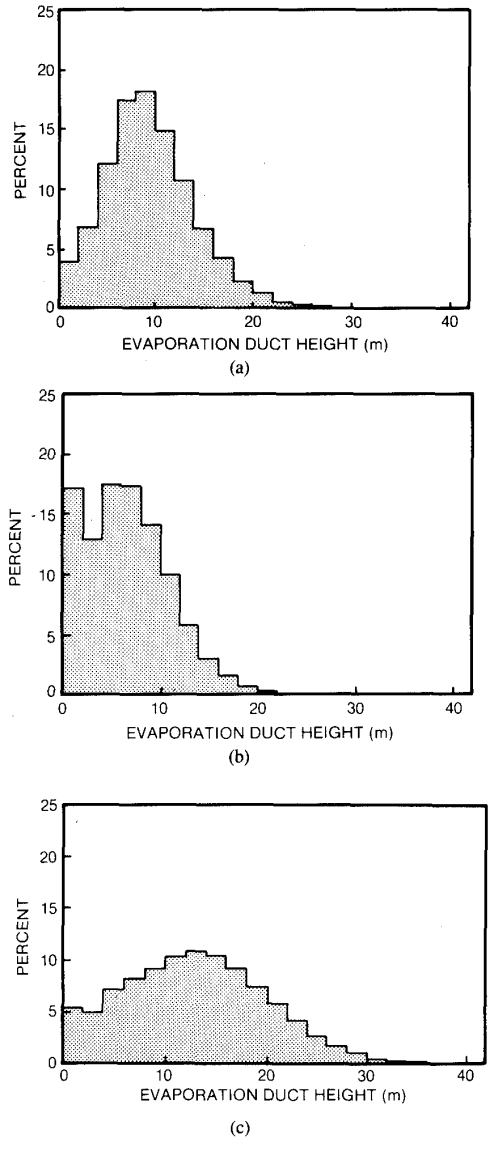

Fig. 3. Yearly mean evaporation duct height distribution for (a) SD site, (b) WC site, and (c) worldwide.

III. Propagation Model

A. Path Loss Calculations

At the ranges of interest, the primary propagation mechanisms in a standard atmosphere are diffraction around the earth and tropospheric scatter. For a transmitter height Z_t and receiver height Z_r in m, the horizon distance H (km) is $H = 3.572((kZ_t)^{1/2} + (kZ_r)^{1/2})$, where k is the effective earth radius factor, 4/3 for a standard atmosphere. Diffraction loss through an evaporation duct can be approximated by a single-mode formulation to the full mode waveguide solution [6] in which the excitation factor and the height-gain functions are expressible in terms of the duct height δ. The path loss is a function of the diffraction loss, the tropospheric scatter loss, and the molecular absorption loss [15]. At a frequency of 16.5 GHz the molecular absorption loss is 0.1 dB/km.

B. Radar Cross Section of Ships

Skolnik [16] empirically relates the average radar cross section of a ship σ_a to the full load displacement in kilotons D and the radar frequency in MHz f by $\sigma_a = 52f^{1/2}D^{3/2}$. The maximum and the minimum radar cross-section varies with aspect angle of incidence and can be approximated by $\sigma_a + 13$ dB and $\sigma_a - 8$ dB [10], [17]. Assuming that the typical surface target observed during the measurements has a five kiloton displacement, σ_a is 48.7 dBsm. The minimum and maximum σ values, $\sigma_{\min}$ and $\sigma_{\max}$, are 40.7 and 61.7 dBsm.

A model of the vertical distribution of cross section is shown in Fig. 4 [10]. The ordinate is the height above the ship's waterline, and the abscissa is a weighting factor $W(z)$, normalized such that the integral over height is unity. Significant radar return is expected only from the ship's superstructure, which is marked by the two height reference lines. These lines allow the model to adapt to various sized ships. In the following analysis, the target superstructure is assumed to be between 9 and 20 m. This appears to be a reasonable height range for the types of ships observed in the measurements.

C. Radar Detection Ranges

The radar equation can be written as

$$P_r = \frac{P_t(G\lambda)^2}{(4\pi)^3 R^4}\,\sigma_a \int W(z)(F(z))^4\,dz \qquad (1)$$

where $F(z)$ is the pattern propagation factor defined as the ratio of the electric field to the free-space electric field at range R [18] and $W(z)$ is the cross section weighting factor from Fig. 4.

Fig. 5 is the path loss at the SD site for a standard atmosphere ($\delta = 0$) and for δ of 2 through 18 m. The three reference lines, labeled MIN, AVG, and MAX, are the path loss thresholds for target cross sections corresponding to $\sigma_{\min}$, σ_a, and $\sigma_{\max}$. When path loss is less than a reference, sufficient power is received by the radar to detect the target; hence, the range at which the path loss curve crosses the threshold is the maximum detection range R_m. Tables II and III list the predicted R_m for the SD and WC sites. The first column is the duct height; the next three columns are the ranges corresponding to target cross sections of $\sigma_{\min}$, σ_a, and $\sigma_{\max}$. Detection ranges for δ greater than 16 m are equal to the value at 16 m because the modes are well trapped.

The R_m predicted for the SD site are, over a narrow range of δ, greater than the R_m predicted for the WC site, even though the latter antenna is higher. In fact, the greatest detection range is for a δ of 10 m at the SD site. The relationship of R_m to the height of the transmitter antenna is complicated. Generally, the lower the transmitter antenna, the greater the R_m becomes for a narrow range of duct heights; conversely, outside this range of δ, the lower the antenna, the lower the R_m. Richter [5] concluded that the optimum location for an antenna is as high as possible above the surface.

IV. Results

Typical radar measurements made during a period when the evaporation duct was the dominant propagation mechanism

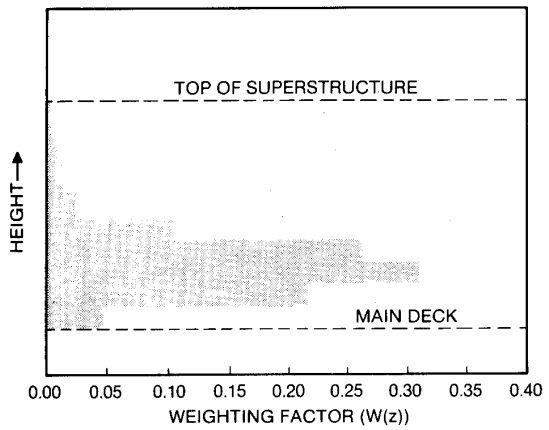

Fig. 4. Radar cross section weighting factor height distribution.

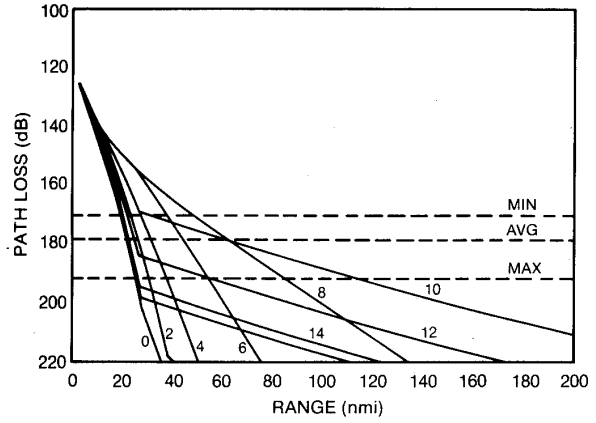

Fig. 5. Maximum detection range for a standard atmosphere (0) and evaporation duct heights from 2 to 18 m. San Diego site.

TABLE II
MAXIMUM SURFACE SHIP DETECTION RANGES PREDICTED FOR DUCT HEIGHTS OF 0 (STANDARD ATMOSPHERE) TO 18 m THICKNESS, SAN DIEGO SITE

Duct Height (m)	Target Cross Section σ_{min}	σ_a	σ_{max}
0	20.0	22.0	25.3
2	23.4	26.2	30.1
4	27.9	31.4	37.1
6	37.8	43.9	53.8
8	49.2	62.6	85.1
10	31.3	59.2	113.6
12	20.6	22.9	51.3
14	19.3	21.0	24.1
16	19.0	20.6	23.4
18	19.0	20.6	23.4

are shown in Fig. 6. This "B-scope" presentation is a composite of 40 radar scans made at the SD site on October 1, 1984 from 1019 to 1159 PST. Five surface ship tracks are indicated (gaps in the tracks are due to computer operations.) The maximum observed detection range is 35 nm, which is approximately 15 nm beyond the standard radio horizon. The highest peak on San Clemente Island (SCI) is 600 m and is just beyond the horizon; however, return from a large portion of

TABLE III
MAXIMUM SURFACE SHIP DETECTION RANGES PREDICTED FOR THE WASHINGTON COAST SITE

Duct Height (m)	Target Cross Section σ_{min}	σ_a	σ_{max}
0	22.7	24.6	27.9
2	25.8	28.8	32.7
4	29.9	33.5	39.2
6	39.0	45.0	54.9
8	48.5	61.9	84.4
10	28.2	55.1	108.9
12	23.2	25.5	47.5
14	22.1	23.8	26.7
16	21.9	23.5	26.1
18	21.9	23.5	26.1

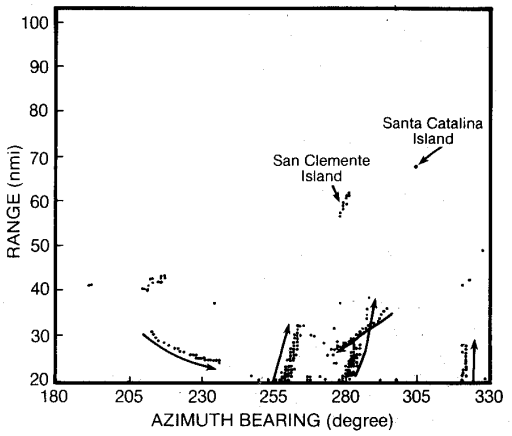

Fig. 6. Radar observations at the SD site on October 1, 1984. Evaporation ducting was the dominant propagation mechanism.

SCI is observed. Santa Catalina Island is lower in maximum elevation than SCI, yet return is observed in one range cell. Also note that the ordinate begins at a range of 20 nm, which is 9 nm beyond the range at which the beam strikes the ocean surface.

Fig. 7 presents the data from a period during which the dominant propagation mechanism was a vertically thick and laterally heterogeneous duct formed from an elevated trapping layer. Radiosonde observations at the SD site indicated an elevated duct (top at 532 m, base at 226 m), whereas observations made on SCI indicated a duct extending from the surface to an altitude of 417 m. Around bearing 220°, a large surface ship and its escort are tracked from an initial range of $\approx$85 nm to a range of $\approx$97 nm, more than four times the standard horizon range. Tracks of three other ships operating near the islands are shown. At a range of greater than 100 nm, Santa Barbara Island is clearly defined; it is approximately 1 square mile in area and well beyond the horizon. Heavy return around bearing 320°, at ranges greater than 60 nm, is from the California coast north of the site.

The two dashed tracks in Fig. 7 are known surface ships that were not tracked by the radar. It is interesting to note that the two ships closest in range were not tracked while ships at longer ranges were successfully tracked. The explanation for this is best visualized by examining the ray trace shown in Fig.

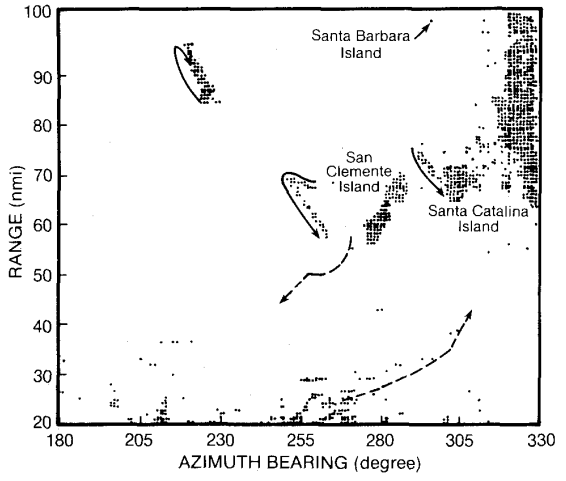

Fig. 7. Radar observations at the SD site on August 24, 1984. Ducting conditions were an elevated duct at the radar gradually decreasing in altitude with increasing range until a surface-based duct formed at San Clemente Island.

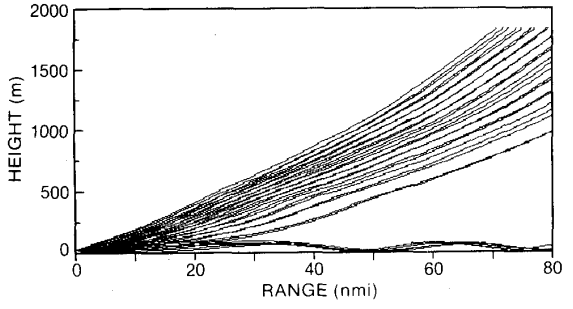

Fig. 8. Raytrace for the laterally heterogeneous ducting environment of August 24, 1984.

8, which takes into account the observed laterally heterogeneous ducting environment. The rays trapped in the elevated duct remain trapped as the duct lowers to the surface. In the range between 20 and 45 nm, the rays are above the surface, creating a skip zone. Very few radar hits are seen along the tracks for the two ships in this area, which is consistent with the ray trace picture. At greater ranges, additional skip zones are shown, yet surface targets are tracked. This is possibly due to scattering of energy in different directions when the ray strikes the surface and some of the scattered energy remains trapped within the surface-based duct. The PC-compatible program for computing this ray trace was developed by Patterson [19].

Figs. 6 and 7 are typical of the measurements; however, individual cases will be put aside, and the focus will be directed to the validation of the propagation model. With the δ distribution and the predicted detection ranges, it is a simple matter to create a distribution of detection ranges. For example, in San Diego, δ between 6 and 8 m are observed 17.4 percent of the time. From Table II, using the σ_a values, the maximum detection range R_m for a δ of 6 m is 43.9 nm; for an 8 m δ, R_m is 62.6 nm. Therefore, detection ranges between 43.9 and 62.6 nm should be observed at least 17.4 percent of

TABLE IV
CUMULATIVE FREQUENCY DISTRIBUTION OF DETECTION RANGES PREDICTED FOR THE SAN DIEGO AND WASHINGTON COAST SITES, TARGET CROSS SECTION IS σ_a

Range (nm)	San Diego	Washington
25	69.8	88.8
30	61.5	66.4
35	54.1	53.1
40	47.2	43.9
45	40.4	34.8
50	33.7	28.0
55	27.0	21.2
60	16.5	6.0
65	0.0	0.0

the time. In practice, 5-nm intervals were selected to distribute the percent occurrence of R_m. Ranges between 50 and 55 nm, for example, are predicted for δ between 6 and 8 m as well as for δs between 10 and 12 m. The percent occurrence of δ between 6 and 8 m, 17.4 percent, is multiplied by 0.266 (the portion of the predicted range within the range interval) and added to the percent occurrence of δs between 10 and 12 m, 14.9 percent, multiplied by 0.137 (the portion of the predicted range within the same range interval). This linear distribution of the percent occurrence is justifiable considering the large number of samples in the δ distribution and the small δ interval of 2 m.

Table IV is the cumulative frequency distribution of R_m for the SD and for the WC sites. These entries are computed for the average target cross section and distributed as described above for the duct height distributions at each site. In San Diego, detection ranges greater than 25 nm are predicted to occur 69.8 percent of the time; ranges greater than 40 nm (nearly twice the standard radio horizon) are predicted to occur 47.2 percent of the time. At the WC site, the standard horizon is 24.6 nm; detection ranges greater than this are predicted 88.8 percent of the time.

Table V is a chronology of the maximum detection range and the type of atmospheric condition observed (locally) at both sites. The condition descriptors are *std*, meaning a standard atmosphere (the evaporation duct is the dominant propagation mechanism); *sbd*, meaning that a surface-based duct was observed during the radar operations; and *elv*, meaning that an elevated duct was present. Of the 36 days, 19 days of measurements were free from contamination by surface-based or elevated ducts.

The effects of the three ducting mechanisms are shown by Fig. 9 in which the detection ranges are grouped by the atmospheric condition descriptor. The reference line labeled Horizon corresponds to the standard radar horizon range for the $\sigma_{\min}$ target at the SD site. Detection ranges during surface-based ducting conditions are consistently greater than three times the horizon range. Although the greatest detection range observed is when an elevated duct is present, the spread in range is large, possibly indicating heterogeneity of the local air masses. Under so-called standard atmospheric conditions, detection ranges greater than or equal to the horizon range are

TABLE V
MAXIMUM DETECTION RANGES OBSERVED DURING THE EXPERIMENT

San Diego Site								
Date	Range	Cond	Date	Range	Cond	Date	Range	Cond
07/03/84	30	std	07/09/84	70	sbd	07/11/84	110	elv
07/12/84	105	sbd	07/23/84	40	elv	07/24/84	85	elv
07/25/84	85	sbd	08/20/84	42	elv	08/21/84	45	elv
08/22/84	40	elv	08/23/84	85	sbd	08/24/84	97	sbd
10/01/84	35	std	10/02/84	50	elv	10/03/84	45	std
01/07/85	20	std	01/08/85	42	std	01/14/85	95	elv
01/22/85	20	std	01/23/85	45	std	01/30/85	50	std
03/04/85	35	std	03/04/85	51	std	03/14/85	32	std
03/19/85	37	std	03/28/85	45	std	04/19/85	42	std
Washington Coast Site								
Date	Range	Cond	Date	Range	Cond	Date	Range	Cond
08/25/85	72	elv	08/26/85	60	std	10/28/85	32	std
10/29/85	38	elv	10/30/85	42	std	12/04/85	50	std
12/07/85	45	std	01/10/86	22	std	01/11/86	35	std

Atmospheric conditions are std, standard atmosphere; sbd, surface-based duct; and elv, elevated duct.

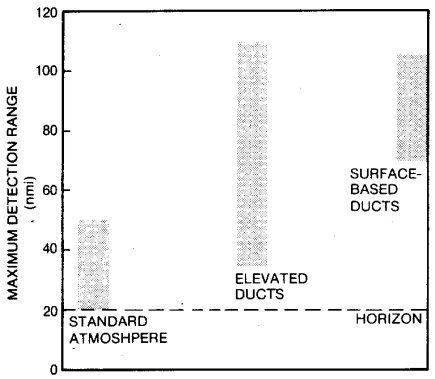

Fig. 9. Observed maximum detection range for the local ducting conditions measured at the radar.

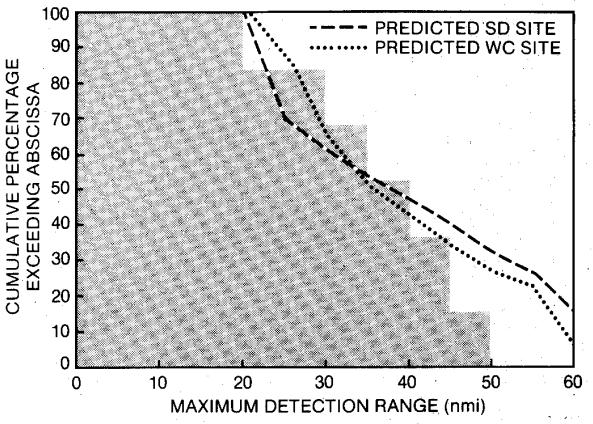

Fig. 10. Comparison of predicted to observed maximum detection ranges during evaporation ducting conditions.

always observed. From the data, the evaporation duct is capable of extending the detection range to more than twice the horizon. In two measurement periods, one at the SD site and one at the WC site, ships were detected at a range of 50 nm, approximately 30 nm beyond the horizon.

Fig. 10 is the cumulative probability distribution of R_m observed at both the SD and WC sites during periods when the evaporation duct is the controlling propagation mechanism (the days tagged with a std condition). Superimposed on the distribution are the maximum ranges predicted from the duct height climatologies. As seen, the predictions agree well with the observations to ranges of less than 45 nm. Beyond 45 nm, the predictions overestimate the probability; however, considering the limited sample size (19 cases), the unknown size of most of the ship targets of opportunity, and the unknown aspect angle, these discrepancies are well within expectations. Considering that the detection range predicted for a standard atmosphere is ≈ 20 nm, the propagation model examined here is clearly the better predictor.

V. Conclusion

Results from an experiment with a shipboard-height 16.5-GHz surface-search radar clearly demonstrates that the evaporation duct supports high signal strength propagation to ranges exceeding twice the standard horizon range. In 19 days of operations, during which the evaporation duct was the dominant propagation mechanism, ship targets were always detected at ranges equal to, and generally greater than, the horizon. Although an extremely conservative estimation of detection range can be made by the assumption of a standard atmosphere, or a 4/3 earth model, this so-called standard atmosphere rarely exists in a maritime environment; predictions based on this assumption can be well off the mark, depending on the geographical location. Additional effects from the presence of surface-based and elevated ducts, observed in nearly half of the measurements, add to the inadequacy of the 4/3 earth model.

Consideration of atmospheric conditions should play a

crucial role in the design of new maritime radar systems. With the validation of the theoretical propagation model, radar system performance in various ocean areas throughout the world can be readily and accurately predicted from an existing climatology of evaporation duct height.

References

[1] B. R. Bean and E. J. Dutton, *Radio Meteorology*. New York: Dover, 1968.

[2] H. V. Hitney, J. H. Richter, R. A. Pappert, K. D. Anderson, and G. B. Baumgartner, Jr., "Tropospheric radio propagation assessment," *Proc. IEEE*, vol. 73, no. 2, pp. 265–283, Feb. 1985.

[3] M. Katzin, R. W. Bauchman, and W. Binnian, "3- and 9-centimeter propagation in low ocean ducts," *Proc. IRE*, vol. 35, no. 9, pp. 891–905, Sept. 1947.

[4] H. Jeske, "Die Ausbreitung elektromagnetischer Wellen im cm- bis m-Band uber dem Meer unter besonderer Berucksichtigung der meteorologischen Bedingungen in der maritimen Grenzschicht," *Hamburger Geophys. Einzelschriften*, Hamburg, DeGruyter and Co., 1965.

[5] J. H. Richter and H. V. Hitney, "The effect of the evaporation duct on microwave propagation," Naval Electron. Lab. Cen. Tech. Rep. 1949, Apr. 1975.

[6] H. V. Hitney, "Propagation modeling in the evaporation duct," Naval Electron. Lab. Cen. Tech. Rep. 1947, 33 pp., Apr. 1975.

[7] R. A. Paulus, "Practical application of an evaporation duct model," *Radio Sci.*, vol. 20, pp. 887–896, 1985.

[8] W. L. Patterson, "Comparison of evaporation duct and path loss models," *Radio Sci.*, vol. 20, pp. 1061–1068, 1985.

[9] L. P. Yeh, "Simple methods for designing troposcatter circuits," *IRE Trans. Commun. Syst.*, vol. CS-8, pp. 193–198, 1960.

[10] K. D. Anderson, "Surface-search radar performance in the evaporation duct: Global predictions," Naval Ocean Syst. Cen. Tech. Rep. 923, Oct. 1983.

[11] W. L. Patterson, "Climatology of marine atmospheric refractive effects," Naval Ocean Syst. Cen. Tech. Doc. 573, Dec. 1982.

[12] National Climatic Center, *Tape Data Family 11 Reference Manual*, Asheville, NC, 1968.

[13] K. D. Anderson, "Worldwide distribution of shipboard surface meteorological observation for EM propagation analysis," Naval Ocean Syst. Cen. Tech. Doc. 1150, Sept. 1987.

[14] L. N. Ortenburger, "Radiosonde data analysis II," GTE/Sylvania Inc., Electronics Syst. Group/Western Div., July 1977.

[15] H. J. Liebe, "Modeling attenuation and phase of radio waves in air at frequencies below 1000 GHz," *Radio Sci*, vol. 16, pp. 1183–1199, 1981.

[16] M. I. Skolnik, "An empirical formula for the radar cross section of ships at grazing incidence," *IEEE Trans. Aerospace Electron. Syst.*, p. 292, Mar. 1974.

[17] F. D. Queen and E. E. Main, "Radar cross sections of surface ships at near grazing incidence," Naval Res. Lab. Rep. 7338, Nov. 1971.

[18] D. E. Kerr, "Fundamental concepts," in *Propagation of Short Radio Waves*, D. E. Kerr, Ed. New York: McGraw-Hill, 1951, pp. 27–41.

[19] W. L. Patterson, "A raytrace method for a laterally heterogeneous environment," Naval Ocean Syst. Cen. Tech. Rep. 1180, July 1987.

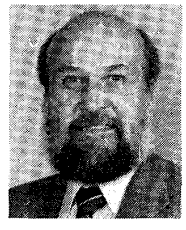

Kenneth D. Anderson was born in San Diego, CA, on May 13, 1950. He received the B.S.E.E. degree from San Diego State University, San Diego, CA, in 1972.

Since graduation he has worked at the Naval Ocean Systems Center, San Diego, where he has been responsible for modeling and measurement programs related to tropospheric propagation effects on naval radar and communication systems. In addition to propagation, his technical interests have been in the development of passive and active atmospheric sensors.